Supporting information

Damage-resistant and healable polyacrylonitrile-derived stretchable materials with exceptional fracture toughness and fatigue threshold

Xiwei Guo[a], Lingqi Huang[a], Jianliang Qin[a], Qi Zhang[a], He Zhu*[a] and Shiping Zhu*[a]

[a] School of Science and Engineering, The Chinese University of Hong Kong, Shenzhen, Shenzhen, 518172, China

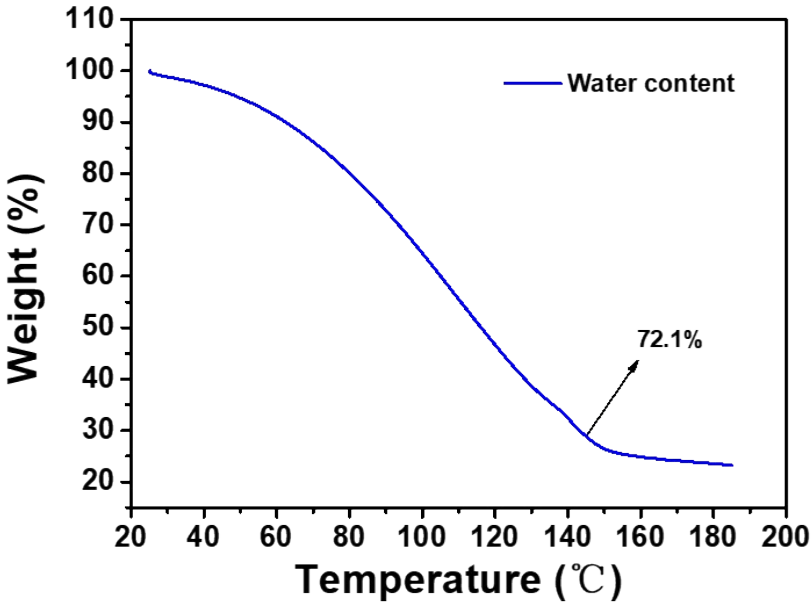

Figure S1. The thermogravimetric analysis (TGA) of water weight percent trapped within APAN.

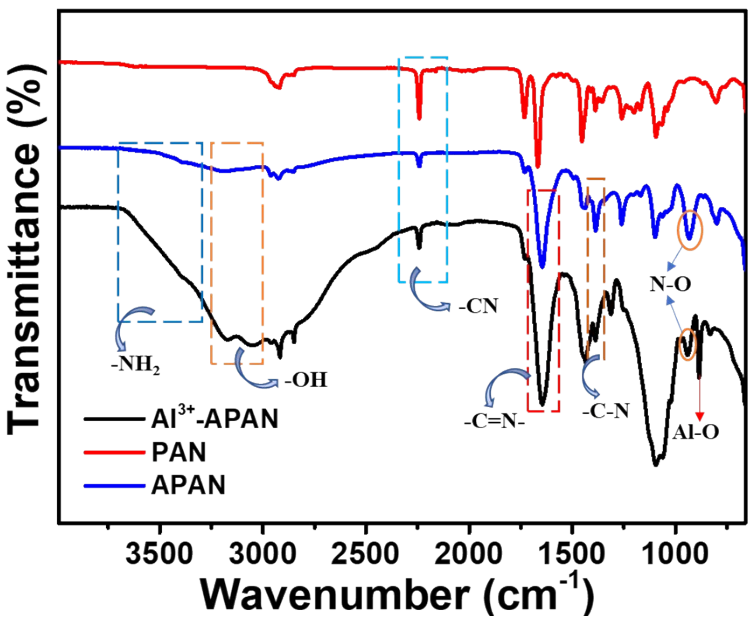

Figure S2. FTIR spectra of PAN, APAN and Al^{3+}-APAN.[1-3] After mixing with Al^{3+}, the absorption peak at 926 cm^{-1} corresponding to N-O group in APAN shifted to a higher wavenumber (943 cm^{-1}) and the absorption intensity of $-NH_2$ was enhanced, indicating the Al-N coordination interaction was formed.[4] Besides, the double-peaks for -OH at 3051 and 3164 cm^{-1}, could be observed, which indicated the presence of both coordinated and uncoordinated -OH groups.[4] Moreover, a new peak for Al-O at

873 cm^{-1} appeared, further suggesting the successful coordination between Al^{3+} and -OH.[5, 6] Therefore, the obtained results demonstrated that the coordination between Al^{3+} and amidoxime group was successfully achieved.

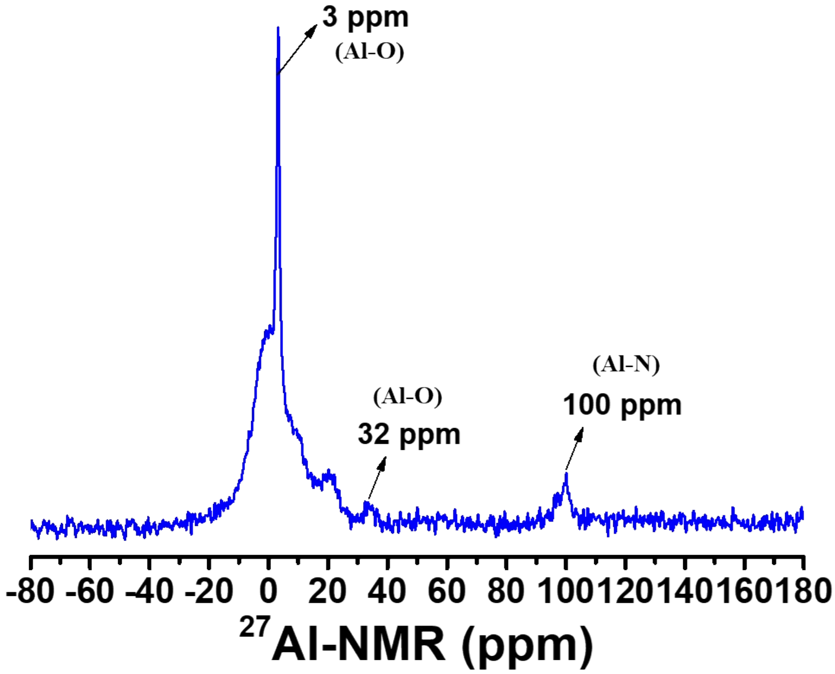

Figure S3. Solid-state ^{27}Al-nuclear magnetic resonance (NMR) spectrum of Al^{3+}-APAN.[4, 7, 8]

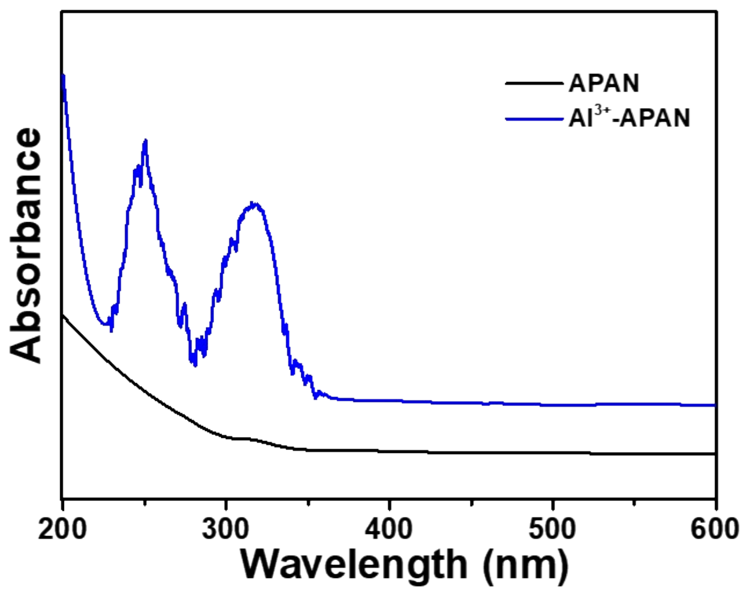

Figure S4. UV−vis spectra of APAN and Al^{3+}-APAN.

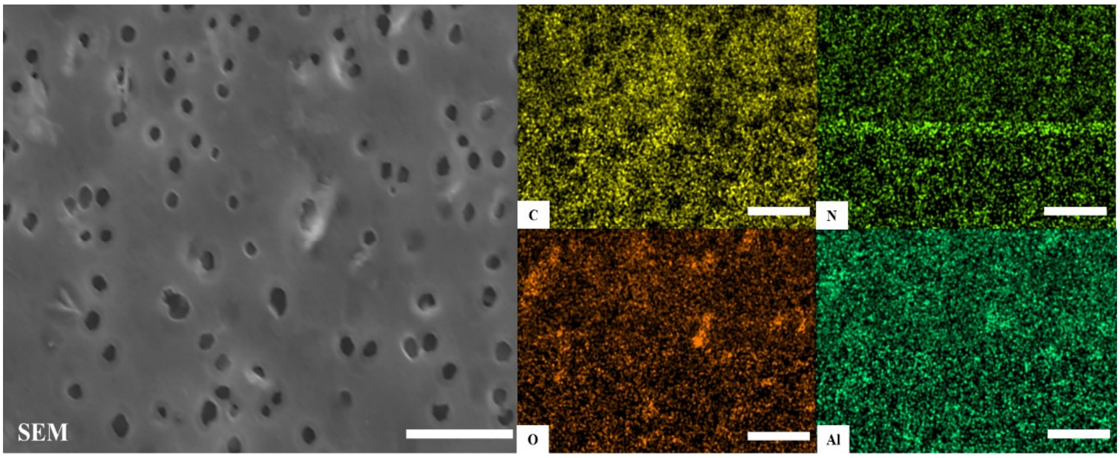

Figure S5. SEM image and its corresponding EDS element maps of the dried Al^{3+}-APAN (the scale bar is 7 μm).

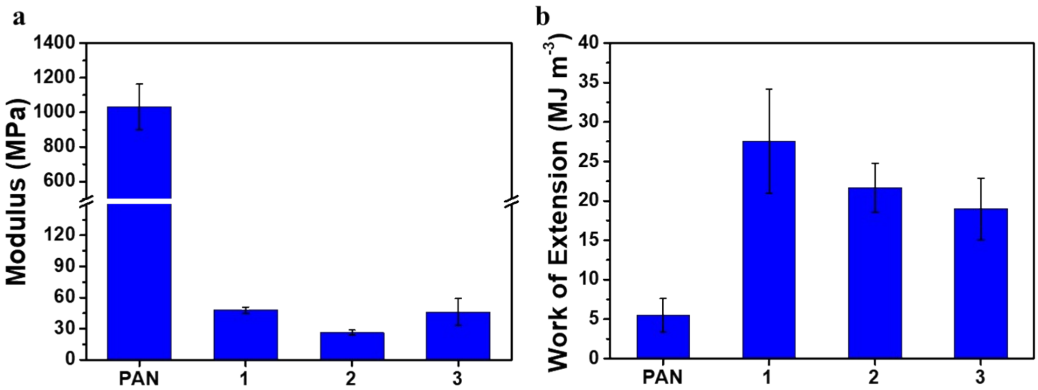

Figure S6. The modulus and work of extension results of PAN, 84 mg Al^{3+}-APAN (1), 126 mg Al^{3+}-APAN (2), and 168 mg Al^{3+}-APAN (3).

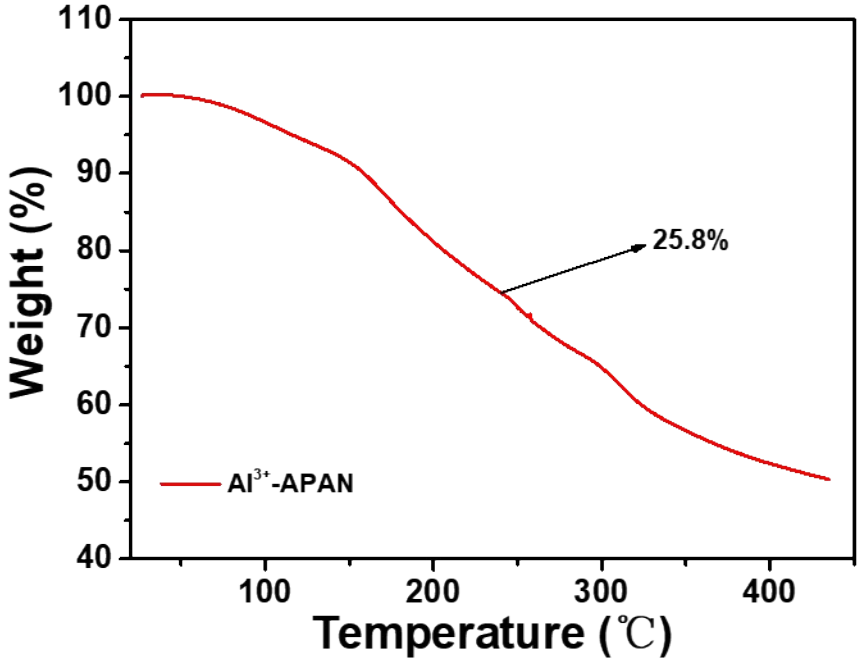

Figure S7. TGA curve of Al^{3+}-APAN. Since the final evaporation temperature of DMF is around 250 °C,[9] the obtained DMF contents for Al^{3+}-APAN, therefore, was about 25.8%.

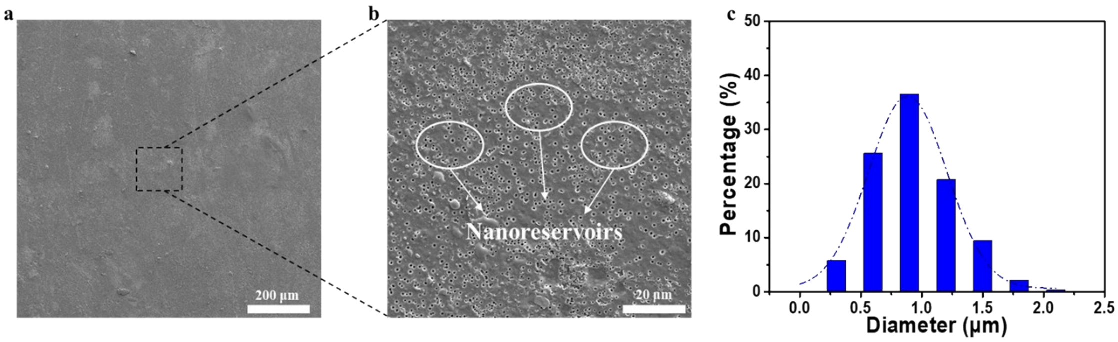

Figure S8. (a) and (b) SEM images of Al^{3+}-APAN, (c) the size distribution of the holes on Al^{3+}-APAN.

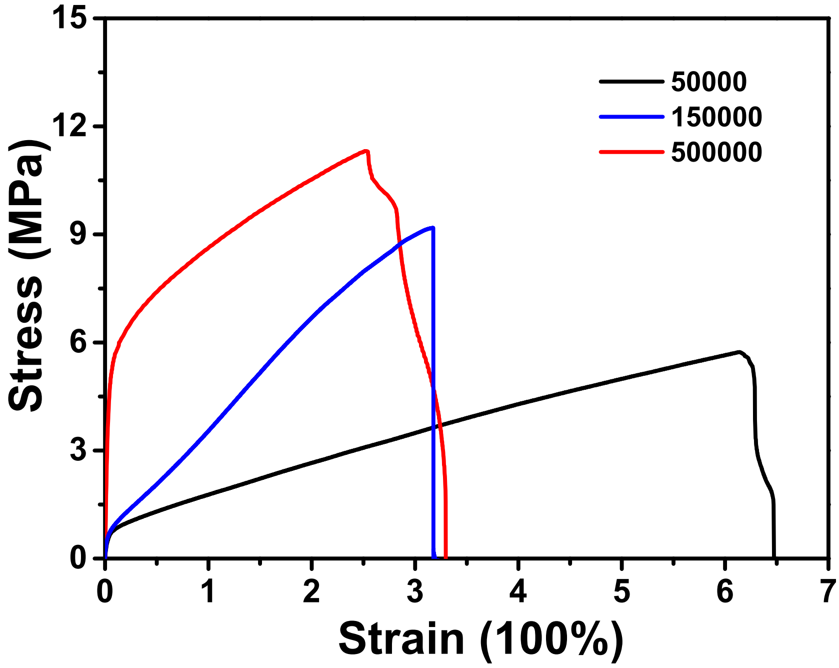

Figure S9. Tensile curves of Al^{3+}-APAN with different molecular weight.

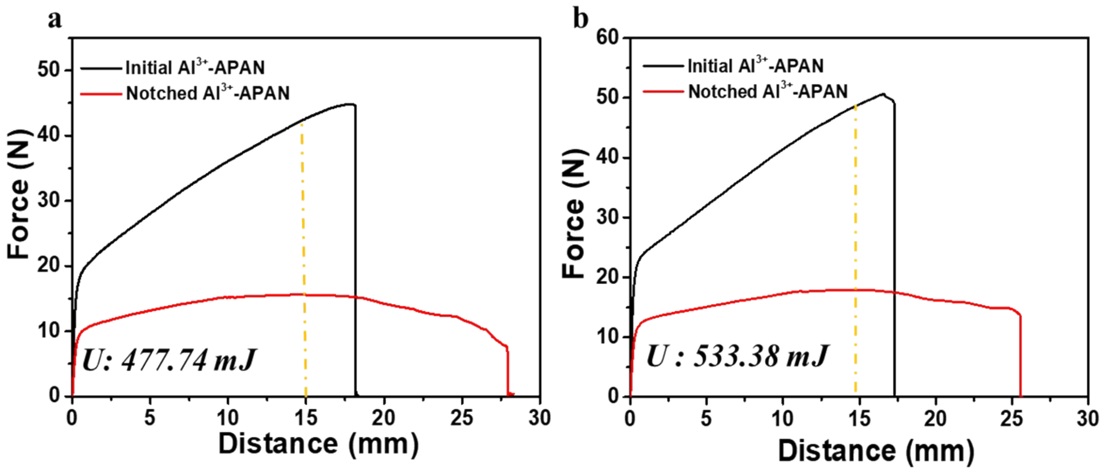

Figure S10. Repeated fracture toughness tests of Al^{3+}-APAN.

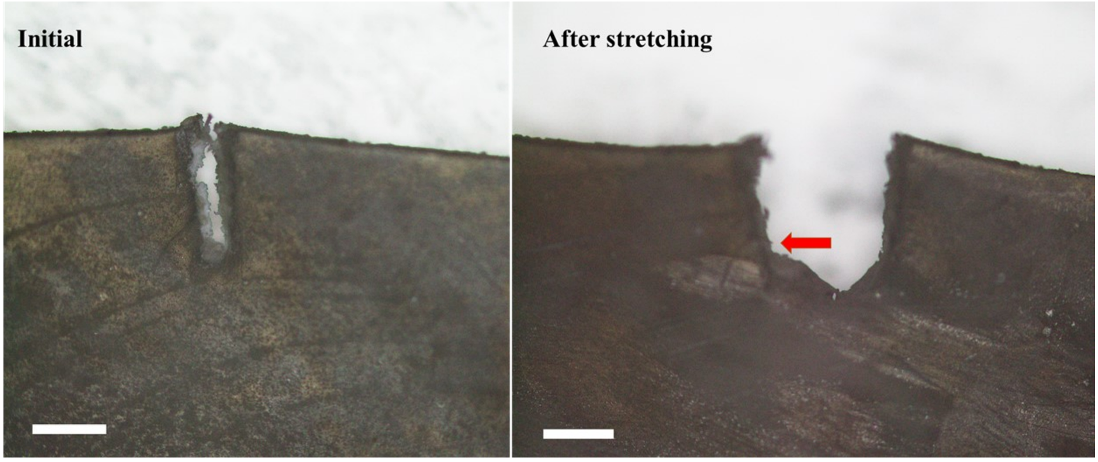

Figure S11. Optical microscopic images of notched Al^{3+}-APAN before and after stretching. The scar bar is 200 μm.

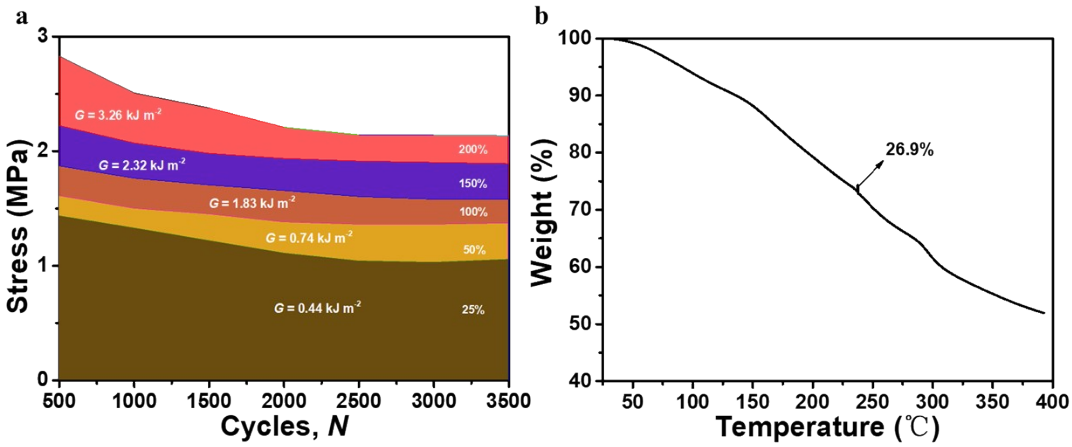

Figure S12. (a) Maximum stress and energy release rate *G* during the cyclic testing of the unnotched samples when loading to 25%, 50%, 100%, 150% and 200% strain for 3500 cycles, (b) DMF content of Al^{3+}-APAN sample after being stretched for 3500 cycles at a strain of 200%, indicating that the content of DMF was generally well-maintained during fatigue test. During cyclic test, the maximum stress of samples after the 2500th cycle generally reached the steady state already. Herein, the stretching curves of the 3000th cycle were used to calculate the *G* values.

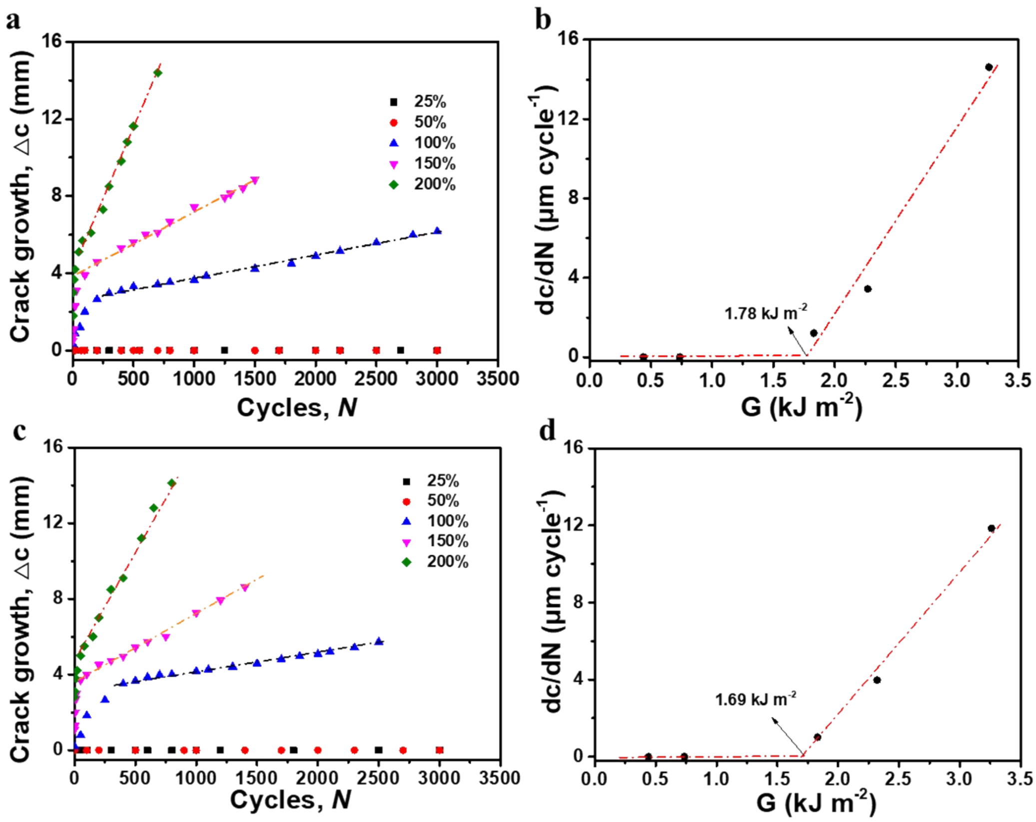

Figure S13. Repeated tests for the determination of fatigue threshold.

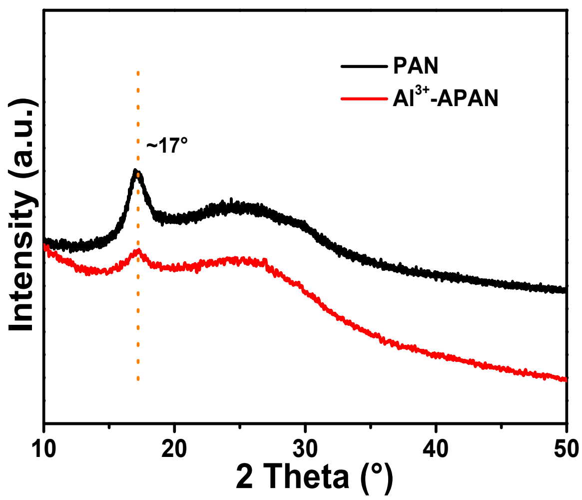

Figure S14. XRD results of pure PAN and Al^{3+}-APAN.

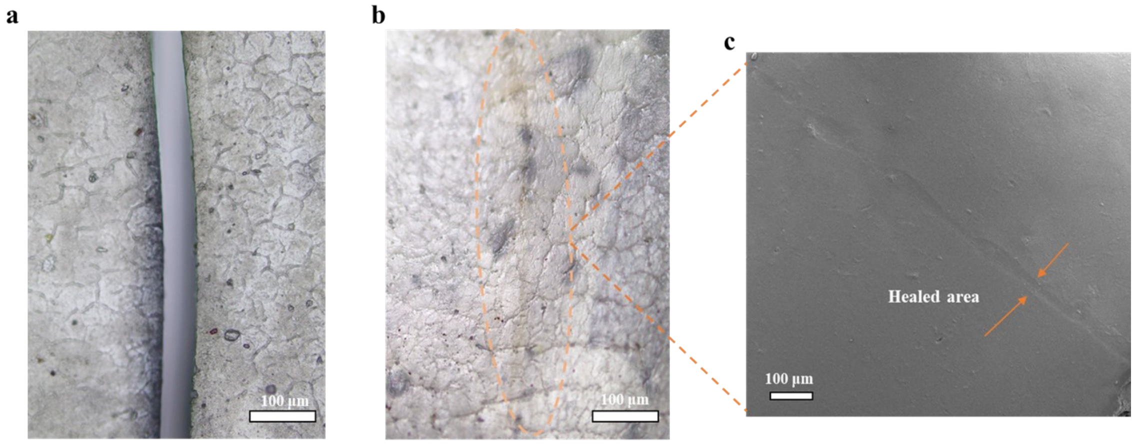

Figure S15. (a) and (b) the optical microscopic images for Al^{3+}-APAN before and after healing for 30 min at 60 °C, and (c) SEM image for the wound of healed Al^{3+}-APAN.

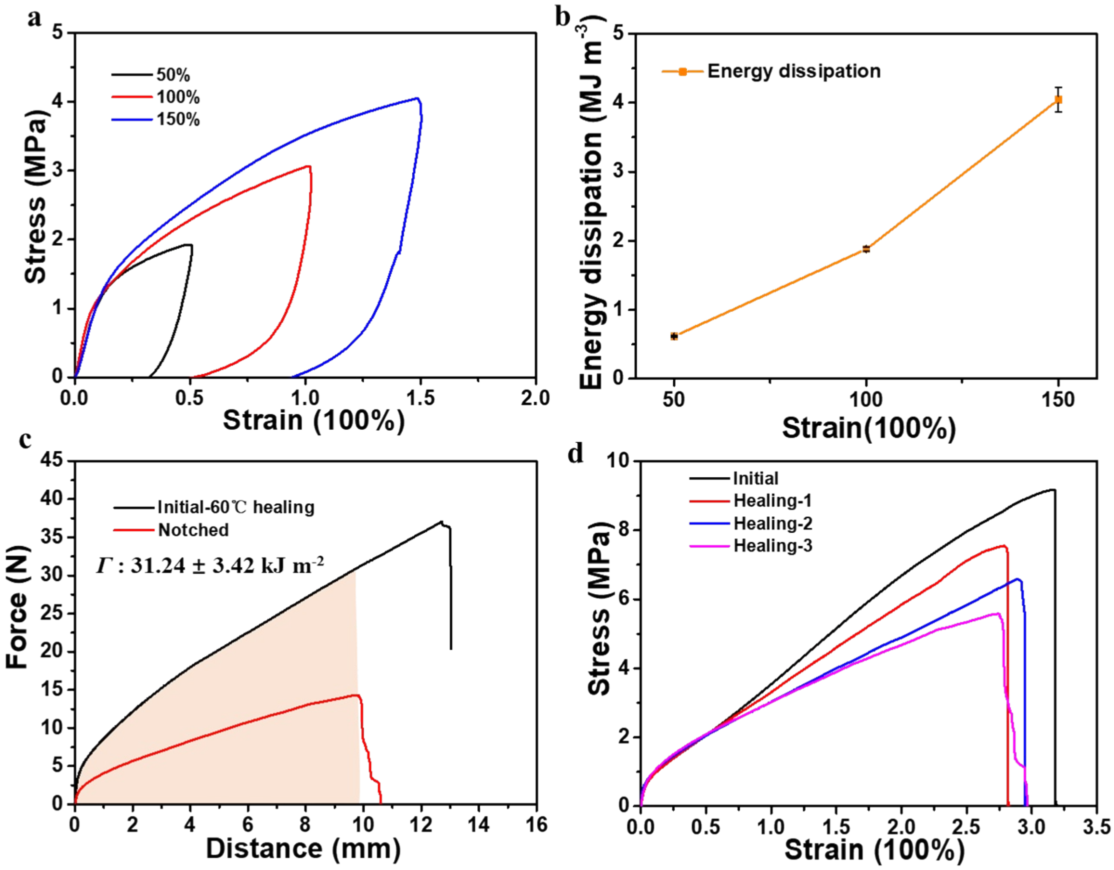

Figure S16. (a) Loading-unloading tests of healed Al^{3+}-APAN at different strains, (b) energy dissipation results at different strains obtained from (a), (c) load-displacement curves from fracture tests of healed Al^{3+}-APAN, and (d) the tensile curves for original and healed Al^{3+}-APAN.

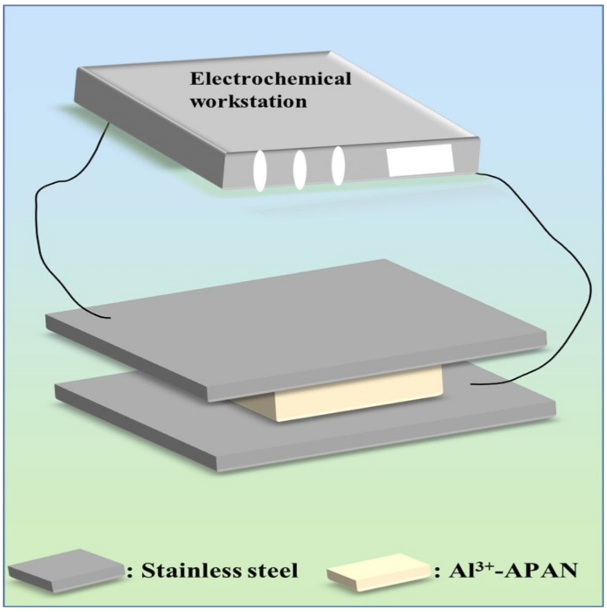

Figure S17. The schematic diagram of impedance spectroscopy test for Al^{3+}-APAN and the conductivity was calculated to be 0.0356 S m^{-1}. The conductivity (δ) was calculated by the following formula: $\delta = L / ((R-R') \times S)$, where R is the resistance of two stainless steels (3.3 Ω) and Al^{3+}-APAN, R' is the resistance of stainless steel, L is the thickness of Al^{3+}-APAN (0.38 mm) and S is the surface area of Al^{3+}-APAN (7.1 mm x 8.0 mm).

References

1. Y. B. Peng, F. Guo, Q. Y. Wen, F. C. Yang and Z. G. Guo, *Sep. Purif. Technol.*, 2017, **184**, 72-78.
2. R. Tan, A. Q. Wang, R. Malpass-Evans, R. Williams, E. W. Zhao, T. Liu, C. C. Ye, X. Q. Zhou, B. P. Darwich, Z. Y. Fan, L. Turcani, E. Jackson, L. J. Chen, S. M. Y. Chong, T. Li, K. E. Jelfs, A. I. Cooper, N. P. Brandon, C. P. Grey, N. B. McKeown and Q. L. Song, *Nat. Mater.*, 2020, **19**, 195-+.
3. X. Guo, C. Zhang, L. Shi, Q. Zhang and H. Zhu, *J. Mater. Chem. A*, 2020, **8**, 20346-20353.
4. Y. Lei, Q. Huang, S. Shan, Y. Lin and A. Zhang, *New J. Chem.*, 2019, **43**, 17441-17445.
5. J. Gangwar, B. K. Gupta, P. Kumar, S. K. Tripathi and A. K. Srivastava, *Dalton Trans.*, 2014, **43**, 17034-17043.
6. R. Romero, V. Ruiz Santoyo, C. Sánchez and M. Rosales, *Nova Scientia*, 2018, **10**, 83.
7. K. J. D. MacKenzie, J. Temuujin, M. E. Smith, K. Okada and Y. Kameshima, *J. Eur. Ceram. Soc.*, 2003, **23**, 1069-1082.
8. J. J. Fitzgerald, S. D. Kohl, G. Piedra, S. F. Dec and G. E. Maciel, *Chem. Mater.*, 1994, **6**, 1915-1917.
9. S. Zhang, A. Hao, Z. Liu, J. G. Park and R. Liang, *Nano Lett.*, 2019, **19**, 3871-3877.